

Active nanoplasmonic metamaterials

O. Hess*, J. B. Pendry, S. A. Maier, R. F. Oulton, J. M. Hamm and K. L. Tsakmakidis

Optical metamaterials and nanoplasmonics bridge the gap between conventional optics and the nanoworld. Exciting and technologically important capabilities range from subwavelength focusing and stopped light to invisibility cloaking, with applications across science and engineering from biophotonics to nanocircuitry. A problem that has hampered practical implementations have been dissipative metal losses, but the efficient use of optical gain has been shown to compensate these and to allow for loss-free operation, amplification and nanoscopic lasing. Here, we review recent and ongoing progress in the realm of active, gain-enhanced nanoplasmonic metamaterials. On introducing and expounding the underlying theoretical concepts of the complex interaction between plasmons and gain media, we examine the experimental efforts in areas such as nanoplasmonic and metamaterial lasers. We underscore important current trends that may lead to improved active imaging, ultrafast nonlinearities on the nanoscale or cavity-free lasing in the stopped-light regime.

The interaction of light with metallic nanostructures and nanoparticles gives rise to a diversity of surprising and profound effects that we have only in recent years begun to fully appreciate, analyse thoroughly and technologically explore^{1,2}. In photonics and optoelectronics, metals were for decades perceived as being rather dull, devoid of interesting or useful optical properties that could be harnessed for optical components and devices. Scientists likewise believed that the wave nature of light imposed seemingly fundamental constraints on the degree to which we can resolve nanoscopic details of an object, or reduce the size of photonic devices. It was the discovery of surface-enhanced Raman scattering^{3–5} in 1974 that drew appreciable attention to the optical properties of metals and, more recently, the pressing need to integrate photonics with nanoelectronics⁶ that propelled metal optics to one of the most actively researched areas of nanoscience and nanotechnology^{7,8}.

The key to the extraordinary optical responses of metals can be traced to the forces that incident light-fields exert on the nearly free (conduction) electrons of a metal, leading to collective electron-photon oscillations that typically occur on scales of just a few tens of nanometres or less, deep below the diffraction limit for visible-light wavelengths ($\lambda \sim 700$ nm). These collective electron-photon oscillations are tightly attached to the surface of a metal, and can be either localized (localized surface plasmons, LSPs) or propagating (surface plasmon polaritons, SPPs). In both forms, they enable a deep-subwavelength localization of incident electromagnetic fields, forming areas of high intensity around plasmonic nanoparticles, as well as allowing for guiding and controlling light below the diffraction limit via SPPs (ref. 7). In addition to nanolocalization of incident light-waves, surface plasmons may efficiently allow for the reverse effect, that is, the out-coupling to the far-field continuum of the near-field of emissive molecules and quantum dots placed adjacently to the metal surface, thereby acting as plasmonic nanoantennas^{9,10}.

When arrays of astutely shaped nanoantennas (each smaller than the wavelength) are assembled in two or three dimensions they may act as the ‘molecules’ or ‘atoms’ of an effective, engineered material — a metamaterial¹¹. The macroscopic optical parameters (effective permittivity, permeability, refractive index, impedance) of such a medium can be made to enter highly unusual regimes, for example, exhibiting a negative refractive index or magnetism at infrared and optical frequencies^{12,13}. This leads to negative refraction

and to completely surprising results, such as the ability of a planar slab of a negative-index (for example, $n = -1$) metamaterial to focus lightwaves without an intrinsic limit to resolution¹⁴, or the possibility to completely stop and localize light pulses in metamaterial and plasmonic heterostructures¹⁵. Even greater control on the propagation of electromagnetic waves is achieved when the meta-atoms are allowed to vary smoothly in all three dimensions according to ‘transformation optics’ design rules, forming anisotropic materials that can, for example, cloak objects of arbitrary shape from incident radiation^{16,17}. Metamaterials have also been shown to allow for an exceptional degree of control on the polarization of light¹⁸, as well as for enhanced nonlinear effects that in some cases can arise entirely from the magnetic field of light^{19,20} — in sharp contrast to nonlinear effects in ordinary optical media, which always arise from the electric field.

The interaction of photons with the conduction electrons of a plasmonic metamaterial gives rise to dissipative optical losses, which for visible light can be significant (of the order of $1,000 \text{ cm}^{-1}$ or more). In essence, there exists a trade-off between localization and loss — the more tightly light fields are localized to the surface of a metal, the higher the fraction of the modal energy is inside the metal, leading to an increase of dissipation as the effective mode volume is reduced²¹. Many envisaged applications can be adversely affected by this inherent feature in the light-plasmon interaction, and although this limitation has been pointed out right from the beginning of plasmonics research^{22,23} it has only recently become possible to identify effective strategies to mitigate losses^{24–27}. One of the most promising is the use of gain materials placed in close proximity to the metal surface^{28–32}. The enhanced electric fields associated with the plasmonic excitations strongly modify the radiative and non-radiative properties of the deployed emitters³³, and for suitably optimized structures loss-free operation^{34–37} or steady-state net amplification³⁸ is possible. Higher gain densities may lead into the lasing regime if both dissipative and radiative losses are overcome^{39–41}. From a theoretical perspective, the complexity of the surface plasmon-gain interactions — both for localized plasmons and propagating SPPs — necessitates the development of sufficiently general theoretical and computational techniques that can aid our understanding of and provide a deeper insight into the involved physics.

In this Review we discuss recent advances in the field of active (gain-enhanced) plasmonic metamaterials, nanocavities and

The Blackett Laboratory, Department of Physics, Imperial College London, South Kensington Campus, London SW7 2AZ, UK.

*e-mail: o.hess@imperial.ac.uk

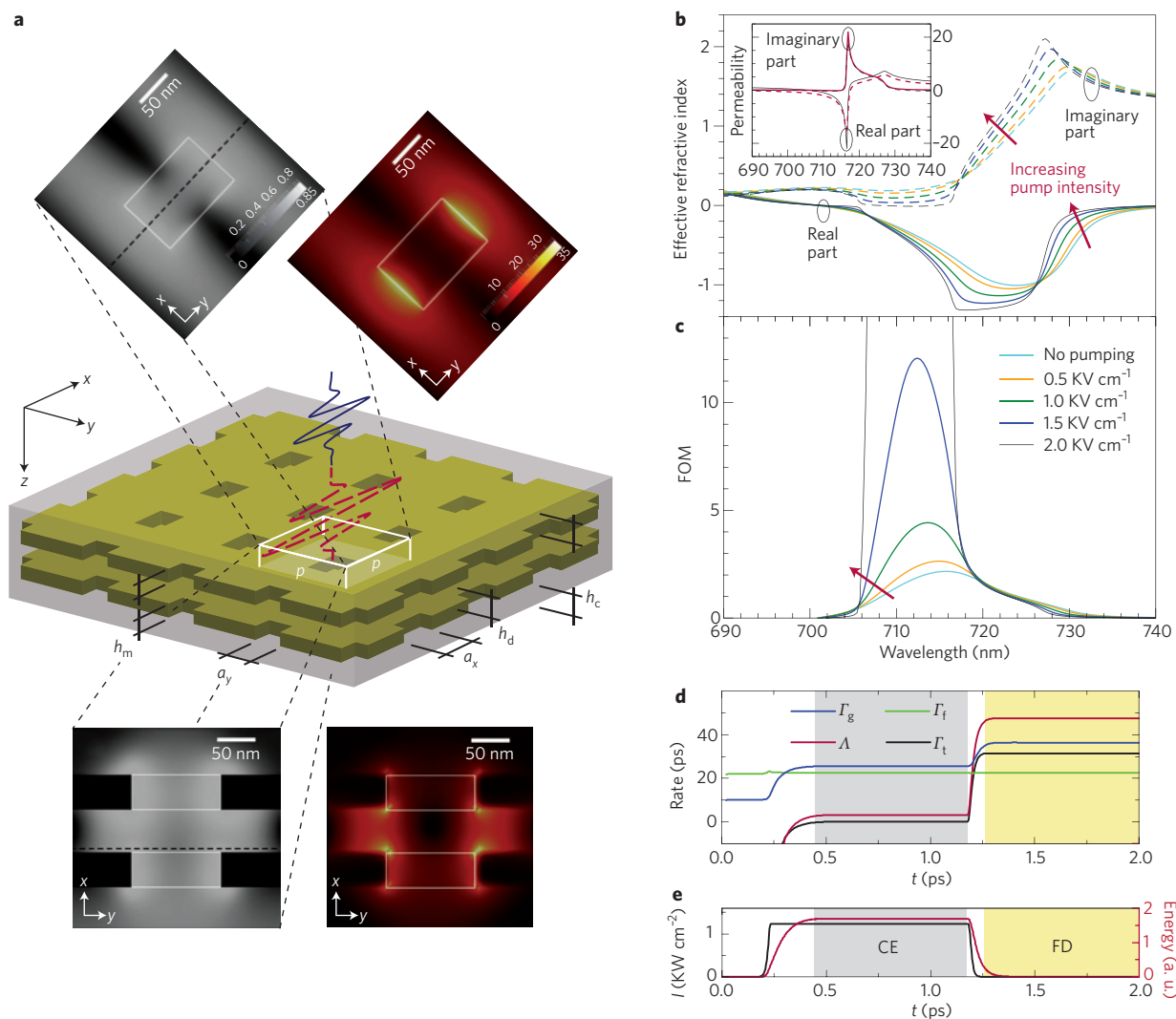


Figure 1 | From loss compensation to steady-state amplification in active negative-index fishnet metamaterials. **a**, Schematic of a dye-doped double-fishnet metamaterial together with exemplary profiles of the inversion (left) and electric-field amplitude (right) at the emission wavelength (710 nm) taken at the xy -plane (top) and zx -plane (bottom). Colour bars: left, light (dark) shades represent high (low) areas of inversion; right, light colours represent the local field enhancement. h_m , h_c and h_d denote the height of the metal, cladding and dielectric layers, respectively; a_x and a_y are the width of the rectangular holes in the x and y direction, p is the periodicity. The incident optical pump and probe pulses are indicated by red and blue waves. **b**, Real and imaginary part of the extracted effective refractive indices n for different pump amplitudes. The peak electric-field amplitude of the pump increases in steps of 0.5 kV cm^{-1} , from no pumping (cyan) to a maximum of 2.0 kV cm^{-1} (black). The inset shows the real and imaginary parts of the effective permeability (black and red lines, respectively) and the corresponding results of Kramers-Kronig calculations (dotted lines) for the highest peak electric-field amplitude of 2.0 kV cm^{-1} . **c**, The figures-of-merit ($\text{FOM} = \text{Re}\{n\}/\text{Im}\{n\}$) for the same pumping amplitudes as those shown in **b**. **d**, Rate dynamics during probing in the amplifying regime of the metamaterial. Shown are the net-gain rate Γ_g (blue), dissipative-loss rate Γ_l (green), outflux/radiative-loss rate Λ (red) and energy-decay rate Γ_t (black). **e**, Dynamics of the probe-pulse intensity I_s (black) and energy U inside the metamaterial (red) in the regimes of continuous excitation (CE) and free decay (FD) for the active optical metamaterial of **d**. Figure reproduced with permission from: **a-c**, ref. 35, © 2010 APS; **d,e**, ref. 38, © 2011 APS.

nanolasers. We begin by concisely reviewing and establishing the general theory that describes gain-assisted plasmonic nanostructures, including metamaterial emitters, nanolasers and so-called spasers, explaining how and why full loss-compensation can be accomplished. We evaluate common treatments of such problems, along with their limitations, and delineate the situations that call for full-wave, spatio-temporally resolved investigations. We then give an overview of recent experimental progress in the construction of loss-compensated negative-index and negative-magnetic metamaterials, as well as plasmonic and metamaterial nanolasers, highlighting the most promising approaches and the further work that remains to be done. Exciting developments pertaining to the use of plasmonic nanocavities and nanoantennas in modifying the

radiative and non-radiative properties of nanoemitters are also discussed. We conclude by providing an outlook of the important challenges that remain to be addressed, such as the reduction of the lasing threshold and the size of the meta-atoms, the areas where the impact from this research is likely to be most tangible, as well as intriguing new directions for the field, including the use of gain in the stopped-light regime.

From loss compensation to amplification

The design of gain-enhanced plasmonic metamaterials having non-trivial three-dimensional (3D) geometries, such as the nano-fishnet^{42,43} or gyrioidal geometries⁴⁴, calls for the development of general, *ab initio* theoretical tools that can faithfully capture the

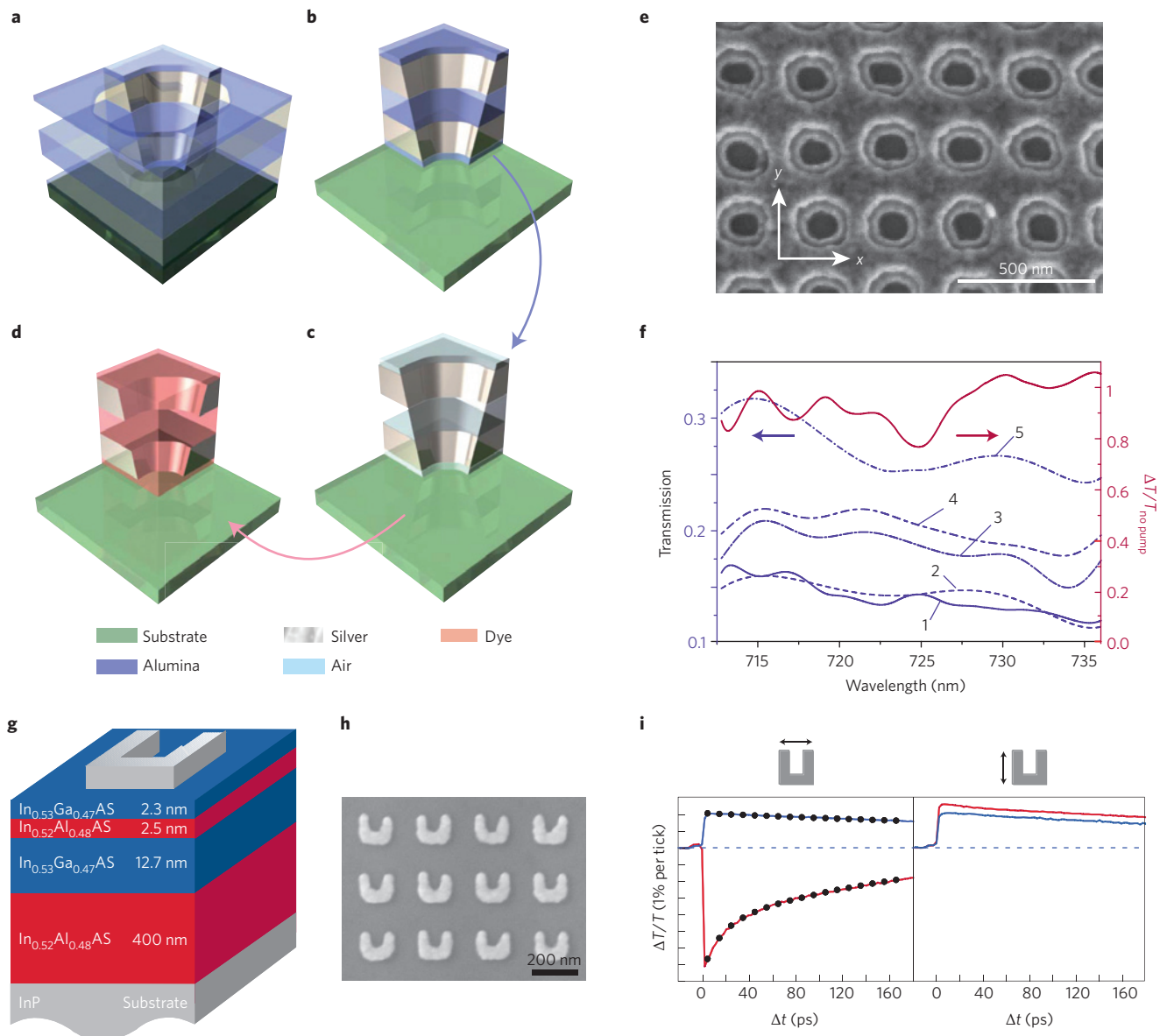


Figure 2 | Experimental demonstration of amplification or loss compensation in gain-enhanced negative-index or negative-magnetic metamaterials. **a-d**, Successive steps in the fabrication of an active negative-refractive-index ‘double-fishnet’ metamaterial. **a**, A unit cell of the structure with the region between the two nanofishnets occupied by alumina. **b**, A quarter of the structure shown sitting on top of an indium tin oxide (ITO)-coated glass substrate. **c**, In this step the alumina spaser is selectively etched out leaving only thin pillars to separate the two nanofishnets. **d**, Finally, the structure of **c** is spin coated with Rhodamine 800 (gain medium), which is deposited in the region between the fishnets and in a thin region above the upper fishnet. **e**, Scanning electron microscope image of the double-fishnet prior to its infiltration with gain. **f**, Experimentally measured transmission coefficients showing how the transmission through the structure progressively increases, from the case (line 1) where there was no prior pumping to the case (line 5) of optimized pump-probe delay (54 ps) and pump power (1 mW). Also shown is the relative transmission change (red), reaching values of the order of 100%, versus wavelength. **g**, A unit cell of an active negative-permeability metamaterial, showing a split-ring resonator grown on top of InGaAs semiconductor QWs. The substrate is InP, the lower barrier is a 400-nm-thick $\text{In}_{0.52}\text{Al}_{0.48}\text{As}$ buffer, the upper barrier is a 2.5-nm-thin $\text{In}_{0.52}\text{Al}_{0.48}\text{As}$ layer (to prevent ‘quenching’ of the gain), whereas the cap 2.3-nm-thin $\text{In}_{0.53}\text{Ga}_{0.47}\text{As}$ layer is used to prevent oxidation of the InAlAs layer underneath it. **h**, Top-view electron micrograph of the grown active nanoplasmic metamaterial. **i**, Measured differential transmittances ($\Delta T/T$) characterizing the active magnetic metamaterial for horizontal (left) and vertical (right) electric-field polarizations. The red lines pertain to the gain-enhanced metamaterial, whereas the blue lines to the bare QW heterostructure. The black dots in the left panel are theoretical fits to the experimental data. The dashed lines indicate zero differential signal transmission. Figure reproduced with permission from: **a-f**, ref. 34, © 2010 NPG; **g-i**, ref. 49, © 2010 OSA.

intricate gain–plasmon interactions, and provide fundamental insight into the dynamical response of the active nanostructures. In addition to allowing for the study of the dynamical interaction between light, surface plasmons and gain molecules/materials, the deployed theory should fulfil the following important prerequisites. First, it should be self-consistent and allow for the modelling of both the pump and probe processes. The latter is necessary to accurately

calculate the spatial profile of the deposited gain inversion during the pump process. Second, the theory should be able to handle nonlinear effects originating from the coherent plasmon–gain interaction, such as gain saturation, gain depletion and spatial hole-burning, which may occur at any point of the 3D geometry. Third, incoherent processes, such as spontaneous emission (SE), should be incorporated in the analysis as they may significantly change not only the

dynamics but also the continuous-wave emission. For instance, SE is sensitive to position within a nanostructure and can distribute among its various spatial modes. Typically, SE close to the metal nanostructure couples preferentially to modes that do not radiate or radiate weakly (so-called dark modes), eventually depleting the gain locally. This spatio-temporal gain depletion may adversely affect the amplification or lasing of the metamaterial's 'bright' modes that are usually studied in reflection and transmission or pump-probe experiments. Thus, both bright and dark modes, as well as SE should be self-consistently treated in the analysis. Finally, the theory should also be able to treat radiation within, transport through and emission from a bulk (larger than the wavelength) metamaterial. Indeed, radiative damping is often the dominant channel in optical metamaterials, and for this reason even perturbative approaches are rather inappropriate, requiring instead a full-wave analysis.

A generic methodology suitable for such investigations is the Maxwell-Bloch approach^{35,37,38,45-47}, augmented with a self-consistent inclusion of Langevin stochastic forces⁴⁰ to incorporate SE noise. This method is computationally intensive but allows for the assessment of realistic, 3D active nanoplasmonic metamaterial structures, larger than the wavelength of incident light. An example of such an active nanostructure, a 'double-fishnet' negative-refractive-index metamaterial, is shown in Fig. 1a. Two 60-nm-thick silver films, perforated periodically with rectangular holes, enclose a thin (60 nm) region infiltrated with Rhodamine-800 dye molecules³⁵. An intense pump pulse of 2 ps duration and centre wavelength of 680 nm, inverts the gain medium. This leads to a 3D occupation inversion profile closely matching the spatial distribution of the electric field at the probe wavelength (710 nm). After 7 ps, a weak broadband pulse of 12 fs duration probes the active structure, and its far-field spectrum is recorded at the two sides of the planar metamaterial. The effective refractive index n of the nanostructure, extracted from the reflection and transmission measurements, together with the associated figure-of-merit ($\text{FOM} = \text{Re}\{n\}/\text{Im}\{n\}$) are shown in Fig. 1b,c, respectively. The insertion of gain results in the imaginary part ($\text{Im}\{n\}$) of n and the absorption coefficient flipping sign in the wavelength regime (around 710 nm) where losses are overcome, as expected. Simultaneously, because of causality and Kramers-Kronig relations (relating $\text{Re}\{n\}$ to $\text{Im}\{n\}$ and vice versa), the real part of n becomes more negative compared with the passive case in the same wavelength region^{35,48}. Note that Fig. 1b also shows that losses are not abolished but spectrally relocated from the negative-index region (~706–718 nm) to regions where $\text{Re}\{n\} > 0$ (for example, $\lambda > 720$ nm).

Fabrication of such an active double-fishnet metamaterial, together with an experimental demonstration (at room temperature) of light amplification in the same structure has been reported by Xiao and colleagues (Fig. 2a–e)³⁴. Here, insertion of a dye-epoxy gain material in the region between two silver fishnets, that is, in the region of highest local fields, ensures optimum harnessing of the available gain (Fig. 1a). A significant enhancement, of the order of 100% in the wavelength range ~715–735 nm, was experimentally observed in the transmission of the probe pulse for optimum level of pumping power and delay between the pump and the probe pulses (Fig. 2f). Note that such a high differential transmittance change $\Delta T/T \sim 1$, sensitive to the polarization and intensity of the pump-probe beams, as well as to their relative time delay, would not have been possible without coupling of the plasmonic metamaterial to the gain medium⁴⁹. By comparison with detailed computational simulations, Xiao and co-workers³⁴ inferred a negative effective refractive index in the region 720–760 nm, with no losses ('negative absorbance') between 722 nm and 738 nm. A major current goal is to fabricate such an amplifying metamaterial and experimentally extract its effective-medium parameters based on the amplitudes and phases of the transmitted and reflected (probe) signals⁵⁰, to unambiguously demonstrate full loss-compensation in the negative-index regime.

Although the use of organic dye molecules, pumped by short optical pulses, provides high gain coefficients and is suitable for proof-of-principle studies, for practical applications it is desirable to deploy solid-state gain materials such as semiconductors, particularly quantum wells (QWs) or quantum dots (QDs)⁴⁵, to supply the necessary gain. Solid-state, semiconductor-based designs allow for potential large-scale integration and can be optically but also electrically pumped (with an injection current). Furthermore, unlike dye molecules that are unstable and photobleach usually within minutes of illumination, semiconductor QWs or QDs are photostable for years, providing robust gain with coefficients that can exceed $1,000 \text{ cm}^{-1}$ (ref. 45). A systematic investigation of QW-based magnetic metamaterials has been reported by Meinzer and co-workers (Fig. 2g–i)⁴⁹. Arrays of silver split-ring resonators (SRRs) were fabricated on top of InGaAs QWs, which were optically pumped at a temperature of 5–10 K.

The relative transmission change (with and without pumping) $\Delta T/T$ of a probe beam was measured for various wavelengths (at 1.48 μm in Fig. 2i) and for both horizontal and vertical polarizations. When the incident probe beam is polarized along the arms of the SRR, that is, when the beam does not couple to the metamaterial, $\Delta T/T$ remains positive (red line in right panel of Fig. 2i) and almost identical to that of the bare QW heterostructure (blue line), never exceeding values of approximately 2.5%. By contrast, when the negative-permeability metamaterial resonance is excited (at which the transmission through the single-negative structure dips), $\Delta T/T$ changes sign (red line in left panel of Fig. 2i), reaching values as low as -8%, while simultaneously the temporal decay of $\Delta T/T$ increases dramatically. These results too, arise owing to the effective coupling of the metamaterial to the gain medium, and owing to the nanoplasmonic Purcell effect — to which we turn our attention in the last two sections of this Review. By engineering the QWs to supply more gain (by a factor of three to four) or by engineering and enhancing the coupling of the QWs to the SRRs, Meinzer and co-workers theoretically show that full loss compensation is within reach.

In all of the above examples, amplification was achieved transiently, using short probe pulses. It is interesting to enquire whether steady-state net amplification is also possible in active nanoplasmonic metamaterials, considering that such a feat is normally prohibited for individual plasmonic nanoparticles (nanoshells, nanospheres and so on) surrounded by gain⁵¹. To this end, we have deployed the Maxwell-Bloch methodology and transformed Poynting's theorem into a global rate-equation problem (Box 1), which allows us to precisely quantify the total-energy decay rate (Γ_t), the net outflux (radiative loss) rate Λ , the plasmonic loss rate (Γ_p), and the absorption in the active medium (Γ_a) and gain (Γ_g) rates³⁸. To reach steady state, the duration of the probe pulse (black line in Fig. 1e) was prolonged until the energy inside the double-fishnet metamaterial became constant with time ($\dot{E}_t = 0$). In that 'continuous excitation' regime, Fig. 1d shows that there is a net outflux ($\Lambda > 0$) of energy through the metamaterial volume, that is, there is more energy radiated away from the volume than energy incident on the volume; hence, we are above the amplification threshold ($\Lambda = 0$).

When the probe pulse is switched off, all rates rebalance into 'free decay' (FD), and the energy inside the active metamaterial now decays exponentially with a rate $\Gamma_t = \Lambda + \Gamma_r - \Gamma_g > 0$. This occurs because there is not sufficient gain (Γ_g) to overcome both the dissipative (Γ_p) and radiative (Λ) losses, that is, to cross the lasing threshold: $\Gamma_g = \Lambda + \Gamma_r$. If, however, sufficient gain is supplied to exceed this threshold, then the energy inside the active nanostructure will start increasing with time until gain depletion sets in — a behaviour that we examine in more detail in the next section. Note that the window over which steady-state amplification can be achieved, between the amplification threshold ($\Gamma_g = \Gamma_r$) and the lasing threshold ($\Gamma_g = \Lambda + \Gamma_r$), is determined by the radiative loss channel (Λ).

Box 1 | Amplification and lasing in nanoplasmonic metamaterials.

To accurately identify the general conditions for amplification and lasing in nanoplasmonic metamaterials we start from Poynting's theorem, according to which we have³⁸:

$$\langle \partial U / \partial t \rangle = -\langle \nabla \cdot \mathbf{S} \rangle - \langle \dot{\mathbf{P}}_f \cdot \mathbf{E} \rangle - \langle \dot{\mathbf{P}}_a \cdot \mathbf{E} \rangle - \langle \dot{\mathbf{P}}_e \cdot \mathbf{E} \rangle \quad (1)$$

where $U(\mathbf{r}, t) = 0.5[\epsilon_p \epsilon(\mathbf{r}) E^2(\mathbf{r}, t) + \mu_0 H^2(\mathbf{r}, t)]$ is the energy density, $\epsilon(\epsilon_0)$ being the local (vacuum) permittivity, μ_0 the vacuum permeability and $\mathbf{H}(\mathbf{r}, t)$ the magnetic field, $\mathbf{S}(\mathbf{r}, t)$ the Poynting vector, $\mathbf{E}(\mathbf{r}, t)$ the electric field and $\mathbf{P}_i(\mathbf{r}, t)$ the polarizations of the free-electron plasma in the metal ($i = f$) and in the gain medium at its absorption ($i = a$) and emission ($i = e$) transitions, and the operator $\langle \rangle$ performs an integration over a volume V and a time averaging that eliminates fast phase oscillations on the scale of the optical frequency. Equation (1) can be recast into the following form:

$$\partial W / \partial t = -\Gamma_t W = -\Lambda W - \Gamma_f W - \Gamma_a W - \Gamma_e W \quad (2)$$

transforming Poynting's theorem into a global rate-equation problem. Here, $W = \langle U + \sum_i w_i \rangle$ is the total field energy that includes contributions from the electromagnetic field energy $\langle U \rangle$ and the energy stored in the polarizations, $\langle \sum_i w_i \rangle$. Further, $\Gamma_t = -(\partial W / \partial t) / W$ is the total-energy decay rate, $\Lambda = \langle \nabla \cdot \mathbf{S} \rangle / W$ the net outflux rate, and $\Gamma_i = [\langle (\partial \mathbf{P}_i / \partial t) \cdot \mathbf{E} - \partial w_i / \partial t \rangle] / W$ are the dissipative ($i = f$), absorption ($i = a$) and gain ($i = e$) rates. Setting $\Gamma_g = -\Gamma_e - \Gamma_a$ we can retrieve the net gain.

When the considered active nanostructure (Fig. B1) is continuously pumped all rates will, at some point, reach steady state, becoming constant with time. Steady-state continuous excitation is characterized by $\Gamma_t = 0$, that is, the volume- and cycle-averaged total field energy inside the metamaterial remains exactly constant with time, owing to a precise balance among all the gain (input and stimulated emission) and loss (dissipative loss, radiative loss and absorption in the gain medium) channels. If dissipative losses are exceeded, there will be more energy exiting volume V than energy entering it (net outflux, $\Lambda = \Gamma_g - \Gamma_f > 0$). Thus, the amplification threshold is: $\Lambda = 0 \leftrightarrow \Gamma_g = \Gamma_f$. With the various rates defined we are able to check whether net amplification ($\Lambda > 0$) is possible in the steady-state regime ($\Gamma_t = 0$) — or whether amplification occurs only transiently⁵¹.

If the excitation is switched off, the energy inside the nanoplasmonic metamaterial will start decaying with a characteristic

rate $\Gamma_t = \omega_e / Q$, with ω_e being the frequency of the excited (for example, negative-index) mode and Q being the metamaterial cavity Q -factor. We are, thus, entering the free-decay (FD) regime. However, if enough gain has been deposited during the pump process, such that the net gain rate (Γ_g) exceeds the sum of the dissipative and radiative losses, $\Gamma_g > \Gamma_f + \Lambda \leftrightarrow \Gamma_t < 0$, then a lasing instability will commence, with the energy inside the active metamaterial increasing with time ($\Gamma_t < 0$) until gain depletion sets in. Thus, the lasing threshold (in the FD regime) is given by $\Gamma_t = 0$.

Note that between the amplification threshold ($\Gamma_g = \Gamma_f$) and the lasing threshold ($\Gamma_g = \Gamma_f + \Lambda$) there is a window, the extent of which is determined by the radiative-loss rate Λ , where steady-state net amplification is possible (free of lasing instabilities). Because practical (transmittive) optical metamaterials are open systems, exhibiting substantial radiative losses, this window is usually broad.

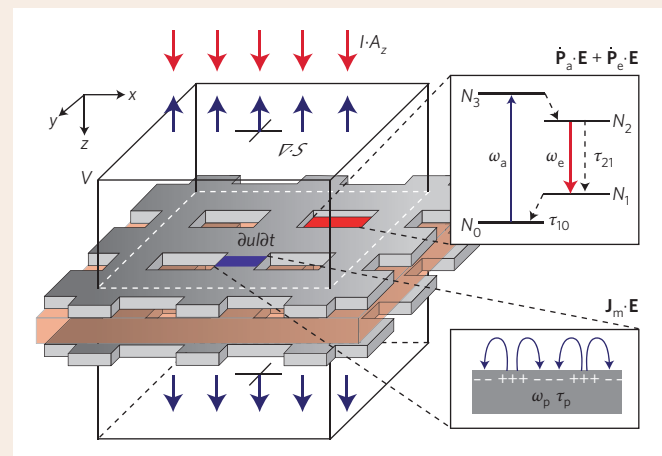


Figure B1 | Loss and gain channels in active metamaterials. Shown are the incident plane wave of intensity I , the net outflux of energy ($\nabla \cdot \mathbf{S}$), the absorption in the metal ($\mathbf{J}_m \cdot \mathbf{E}$) and the absorption (emission) in the gain medium at ω_a (ω_e). The dynamic balance between these channels gives rise to a temporal variation of the total electromagnetic energy u inside the volume V encompassing the metamaterial. A_z is the xy -surface of the volume (shown as an outline of a cube) containing the metamaterial. Figure reproduced with permission from ref. 38, © 2011 APS.

In realistic metamaterials, with unit-cell sizes smaller than the wavelength λ (Box 2) but with overall metamaterial size much larger than λ , radiative losses can exceed dissipative losses (at optical frequencies) by more than a factor of two^{52,53}, as can be seen from Fig. 1d (compare Λ and Γ_f in the FD regime). Therefore, this significant (here, dominant) loss channel clearly cannot be ignored when analysing active nanostructures with dimensions larger than λ . Indeed, without radiation being accurately incorporated into the analysis, for example, within the context of a quasi-static approach where radiation is usually ignored, the two thresholds would seem to exactly coincide, suggesting that only nanolasing but not amplification would be possible^{54,55}. Thus, owing to the significant presence of radiation in nanoplasmonic metamaterials, overcoming dissipative losses and achieving steady-state amplification, that is, operating between the two thresholds, is a realistic possibility, even in the negative-index regime^{56,57}.

Until now, we have discussed how the introduction of gain in a nanoplasmonic metamaterial may lead to amplification of a probe beam^{58–60}. However, when further gain is supplied, it can also lead to

amplification of SE noise within the active metamaterial. Provided that gain is not depleted via other coherent probe beams, eventually a gain instability occurs, leading to laser action^{61–64} at some resonance of the metamaterial. In the next sections we turn our attention to obtaining a deeper understanding and an overview of recent progress on lasing in such systems.

Bright and dark lasing states

When the gain supplied by the active medium embedded within a nanoplasmonic metamaterial is sufficient to overcome dissipative and radiative losses ($\Gamma_g = \Lambda + \Gamma_f$), the energy inside the active nanostructure will start rising with time. At some point (around 18 ps in the example shown in Fig. 3a) the optical field becomes sufficiently strong to undergo a phase transition — an intense lasing burst depleting the available gain^{40,41}. A sequence of damped-amplitude, ‘rise and fall’ relaxation oscillations follows, until the system finds its (quasi-)equilibrium and steady-state lasing emission⁴⁵. During this dynamic start-up phase, both the far-field (bright mode) intensity and the inversion oscillate on a timescale of a few picoseconds,

Box 2 | Gain in metamaterials with deep-subwavelength meta-atoms.

We present a simple, analytic model containing the essential ingredients of gain-enhanced plasmonic metamaterials. Here, the meta-atoms are taken to be deep-subwavelength, allowing for well-defined effective-medium metamaterial parameters. We shall examine whether in this regime there can be extensive regions of operation where stable gain might be possible.

Take a 1D infinite system consisting of a linear array of plasmonic dipole resonators. For simplicity, we consider only one mode per site and assume that the lattice spacing, d , is sufficiently small that only electrostatic interactions matter, and that the system emits no far-field radiation. The amplitude of the electric field on site n is given by α_n , and the field can couple electrostatically through the Förster mechanism to nearest neighbour sites:

$$\omega\alpha_n = \Omega\alpha_n + \eta\alpha_{n+1} + \eta\alpha_{n-1} \quad (3)$$

where Ω is the frequency of the resonance and η is the rate of migration to the neighbouring sites. All these terms are electrostatic in origin and therefore scale-invariant: the size of the unit cell is irrelevant providing it is much less than the wavelength in free space. This equation sustains Bloch wave solutions of the form, $\alpha_n = \alpha_0 \exp(iknd)$, where k is the Bloch wave vector. Substituting into equation (3) gives:

$$\cos(kd) = (\omega - \Omega)/(2\eta) \quad (4)$$

So far we have assumed that all sites are identical but now we introduce some loss on the central site by making the resonant frequency complex, $\Omega_0 = \Omega + i\delta$, where δ denotes the temporal loss, so that a wave incident from $-\infty$ is partly absorbed at the zeroth site, partly reflected and partly transmitted: $\alpha_n = \alpha_0 \exp(+iknd) + R \exp(-iknd)$, for $n < 0$; $\alpha_n = \alpha_0$, for $n = 0$; and $\alpha_n = T \exp(+iknd)$, for $n > 0$; where we have assumed that $kn > 0$. There are three unknowns and we use the following three equations to determine R , T , α_0 : $\omega\alpha_{-1} = \Omega\alpha_{-1} + \eta\alpha_0 + \eta\alpha_{-2}$; $\omega\alpha_0 = \Omega_0\alpha_0 + \eta\alpha_{+1} + \eta\alpha_{-1}$; and $\omega\alpha_{+1} = \Omega\alpha_{+1} + \eta\alpha_{+2} + \eta\alpha_0$, which yields:

$$T = \{1 + \delta/[|2\eta\sin(kd)|]\}^{-1} \quad (5)$$

Hence, as losses increase, transmission decreases.

Next, we introduce some gain onto the zeroth site, $\Omega'_0 = \Omega + i\delta - i\gamma$, where $-i\gamma$ represents the gain. We can easily modify equation (5) to include gain: $T = \{1 + (\delta - \gamma)/[|2\eta\sin(kd)|]\}^{-1}$. Now we see the effect of gain: when $\delta = \gamma$ loss is exactly compensated and unit transmission is retrieved. When $\delta < \gamma$ transmission is enhanced and we have amplified the incident wave. We can also see that when $\gamma > \delta + |2\eta\sin(kd)|$ an instability develops that is the spasing action. Thus, there is indeed a margin of stable amplification:

$$\delta < \gamma < \delta + |2\eta\sin(kd)| \quad (6)$$

There is a simple physical interpretation of this result. The group velocity follows from equation (4): $d(\omega/dk) = dv_g = -|2\eta\sin(kd)|$. Hence, $|2\eta\sin(kd)|$ measures the rate at which energy escapes from a given resonator. The gain has to compensate for, both, the loss in the resonator and for the loss of energy to neighbouring cells through the Förster mechanism.

Some typical numbers for the resonant frequency in plasmonic systems are of the order $\hbar\omega = 2$ eV, $\hbar\eta = 0.5$ eV and $\hbar\delta = 0.2$ eV. Substituting these numbers into equation (6) and assuming a frequency in the middle of the resonant band $kd = \pi/2$: 0.2 eV $< \hbar\gamma < 1.2$ eV. Too much gain drives a localized spasing action, which ultimately leads to local saturation of the gain at the maximum stable level. Below the threshold, amplification is proportional to the gain.

We are also free to introduce feedback, either due to reflectors or the wider plasmonic environment, into the system. The feedback may originate from some distance away from the gain. In this way more conventional lasing action can be generated. We can then distinguish between (near field) lasing and spasing in plasmonic systems: spasing is an instability intrinsic to a metamaterial cell; lasing is a process in which radiation escapes from a stable gain region, but is returned repeatedly to that region by feedback, similar to a conventional lasing system.

giving rise to ultrafast nonlinear responses on the nanoscale with frequencies close to the terahertz regime⁶⁵.

It might be expected that once these oscillations settle down, an undisrupted steady-state emission will ensue (providing pumping continues). However, as mentioned earlier, it is important to recognize that, in addition to bright modes, an active metamaterial also supports dark modes that can deplete the gain, and in some cases even lase themselves. The lasing of dark surface plasmon states is often referred to as ‘spasing’ action^{32,51,55}, as the role of near-field surface plasmons in the amplification and stimulated emission processes dominates. These dark (for example, quadrupole) modes are not, for normal incidence, directly excitable from the outside (though they are excitable for larger incidence angles and diffraction orders) but can be easily excited internally through SE once the gain medium has been pumped to inversion. The bright and dark modes compete for gain and because their dynamics and 3D spatial profiles differ substantially, they can deplete the gain at different times and at different locations. Thus, even if the bright mode crosses the lasing threshold and depletes the gain at areas where its electric field is maximum, there may still be sufficient gain for the dark mode to overcome dissipative losses (radiative losses for a truly dark mode are negligible) and become unstable. This behaviour can clearly be observed in the example shown in Fig. 3, where at around 50 ps a sudden drop is seen in the (emitted) far-field intensity of the bright

mode, while the electric-field intensity of the dark mode (recorded inside the active nanofishnet metamaterial) starts undergoing relaxation oscillations (yellow dash-dotted line in Fig. 3b). The dip in the far-field lasing intensity of the bright mode seen in Fig. 3a is caused by the reduction of the available gain once the dark mode crosses its threshold.

A fundamentally different response can be obtained when the order by which the bright and dark modes exceed their thresholds is reversed. In the example shown in Fig. 3, the cold-cavity resonance frequency of the bright mode is, due to the well-known ‘frequency pulling’ effect⁴⁵, red-shifted from 713.8 nm to 717.25 nm, while the dark mode experiences a blue-shift from 732.2 nm to 731.8 nm — both shifted towards the emission-peak frequency of 718 nm of the gain medium (laser dyes). As can be seen from Fig. 3d,e due to the dark mode’s larger Q factor, spasing can occur even when the emission wavelength of the gain material is close to the bright mode resonance wavelength (713.8 nm) and, here, it can only be completely suppressed if the emission line maximum falls below 715 nm. Above this wavelength, the dark mode gains in strength, while the bright mode increasingly weakens until, at around 720 nm (for E_x pumping, favouring the bright mode) or 725 nm (for E_y pumping, favouring the dark mode), the bright mode eventually switches off. In that region, where the dark mode completely dominates and can deplete the gain at the locations where its field is maximum, it may not be

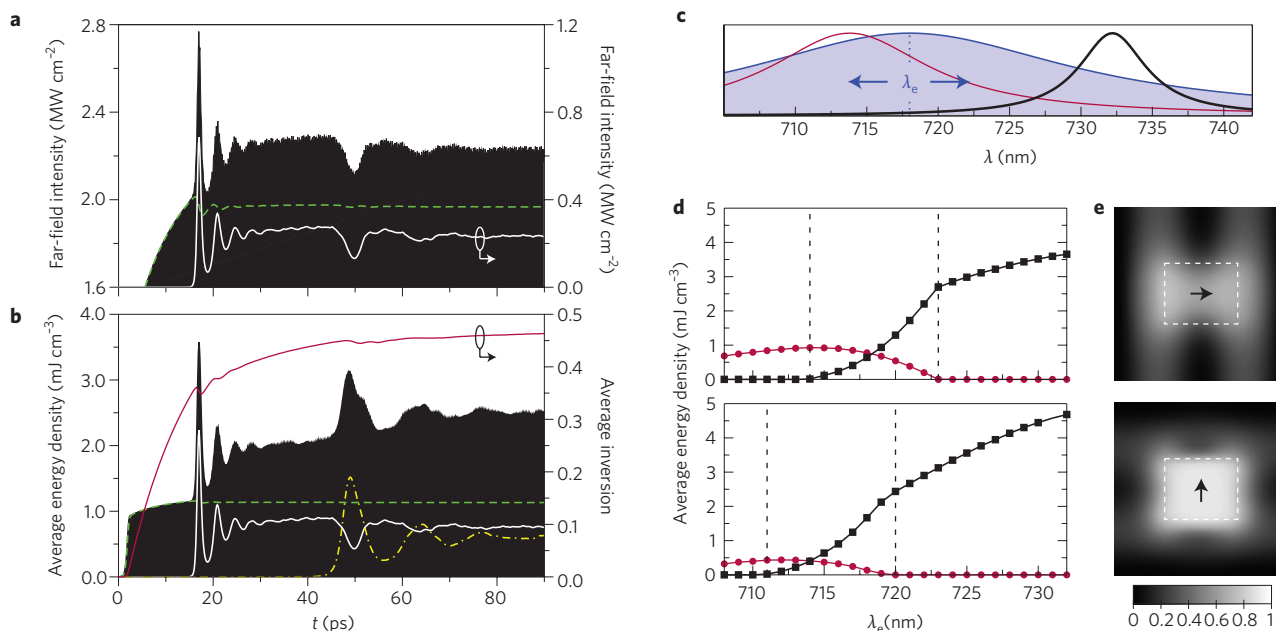


Figure 3 | Dynamics of bright and dark lasing states in gain-enhanced double-fishnets. **a**, Relaxation oscillations in the far-field intensity (black) of the light emitted by the lasing metamaterial. Using a filtering technique^{40,41}, also retrieved and shown are the intensity at the pump wavelength 680 nm (green) and at the bright mode wavelength 717.25 nm (white). **b**, Relaxation oscillations of the average energy density (black) inside the active double-fishnet, together with the corresponding time evolution of the average inversion (red) and the intensities at the pump wavelength (green), bright mode wavelength (white) and dark mode wavelength 731.8 nm (yellow). **c**, Schematic of the emission line (λ_e) together with those of the bright (red) and dark (black) lasing states. The emission line may be shifted to provide control over the lasing state and the polarization of the emissive metamaterial. **d**, Steady-state far-field emission of the bright (red) and dark (black) modes when pumped with E_x (top) or E_y polarization (bottom). The two dashed lines mark the boundaries between the three regimes where there is only the bright mode (left), where the bright and dark modes coexist (middle) and where only the dark mode is present (right). **e**, Inversion profiles before the onset of relaxation oscillations for E_x (top) or E_y (bottom) pumping. The black arrows indicate the polarization of the pump field. The colour bar shows the magnitude of the local inversion. Figure reproduced with permission from ref. 41, © 2012 APS.

possible for the bright mode to even overcome its amplification (loss compensation) threshold. Thus, both of these two methods for mode control (choice of pump polarization and emission-peak frequency of the gain medium) can dramatically affect the active response of a periodic, gain-enhanced nanoplasmonic metamaterial.

An experimental glimpse into the structure of cold-cavity dark and bright states in bowtie meta-atoms is shown in Fig. 4. The dark plasmon modes can be revealed on excitation with electromagnetic fields varying on spatial length scales smaller than the wavelength of free-space radiation. Prominent techniques for these investigations are electron energy-loss spectroscopy (EELS) and cathodoluminescence^{66,67}. As Fig. 4 shows, the EELS technique allows the complete mode mapping of both bright and dark modes⁶⁸ in coupled gold meta-atoms. Besides its importance for the design of optical metamaterials, a thorough understanding of electromagnetic coupling between closely spaced nanoscale metallic elements sustaining localized plasmon modes is also imperative for the design of nano-antennas and nanocavities for light-emission control^{10,33}. Here, the emergence of hybridized modes out of the parent plasmon modes of the respective subunits can be intuitively, and also quantitatively, understood via the plasmon hybridization model⁶⁹.

The existence of dark, nanolocalized modes with negligible dipole moment becomes important when using plasmonic nanocavities as central elements for the control over the radiative properties of nearby active media and light emitters. Recent works have shown that such cavities can be designed to allow for, both, the spectral reshaping of the emission spectrum of light emitters⁷⁰ and the selective removal of unwanted long-lived states of organic light emitters⁷¹. Apart from the plasmon hybridization concept, another prominent tool for radiative-property design are Fano resonances⁷². Here, the coupling of (spectrally broad) dipolar modes with

higher-order dark, and hence spectrally sharp, modes within the plasmonic cavity leads to the suppression of radiative coupling in a narrow frequency range, via linear destructive interference, which can be understood via a Fano-type coupling mechanism^{73,74}.

Nanolasers and coherent metamaterial emitters

Nanoplasmonic and conventional lasers essentially rely on the same physics. However, as we have previously seen, by amplifying optical modes of metallic nanostructures there is the ability to generate and nanolocalize coherent light, rapidly and efficiently, on truly nanoscopic dimensions^{32,39–41}. Despite a number of technical challenges, plasmon and photon lasers have so far shared similar construction principles. Surface plasmons are directly generated on a metal nanostructure and amplified by an adjacent dielectric medium incorporating gain, while a feedback mechanism allows the plasmon cavity modes to resonate. The gain medium amplifies the surface plasmons by stimulated emission of radiation, and in the deep-subwavelength limit the nanolaser may act as a 'spaser'³², a coherent generator of surface plasmons that do not radiate to the far-field.

An important motivation behind spasers is their potential to act as sources that can generate, focus and sustain nanolocalized fields, not directly excitable from free space. Following the external pumping and the creation of inversion in the gain medium, the emitters may couple their energy without radiation to the surface plasmons, which in turn stimulate further radiationless transitions. This provides a mechanism for funnelling energy coherently into a particular mode, on deep-subwavelength scales and without suffering from additional radiative losses. Plasmonic and metamaterial lasers also rely critically on stimulated emission by plasmonic excitations, but unlike spasers these excitations are usually bright (see previous section), the structures are not necessarily deep-subwavelength in

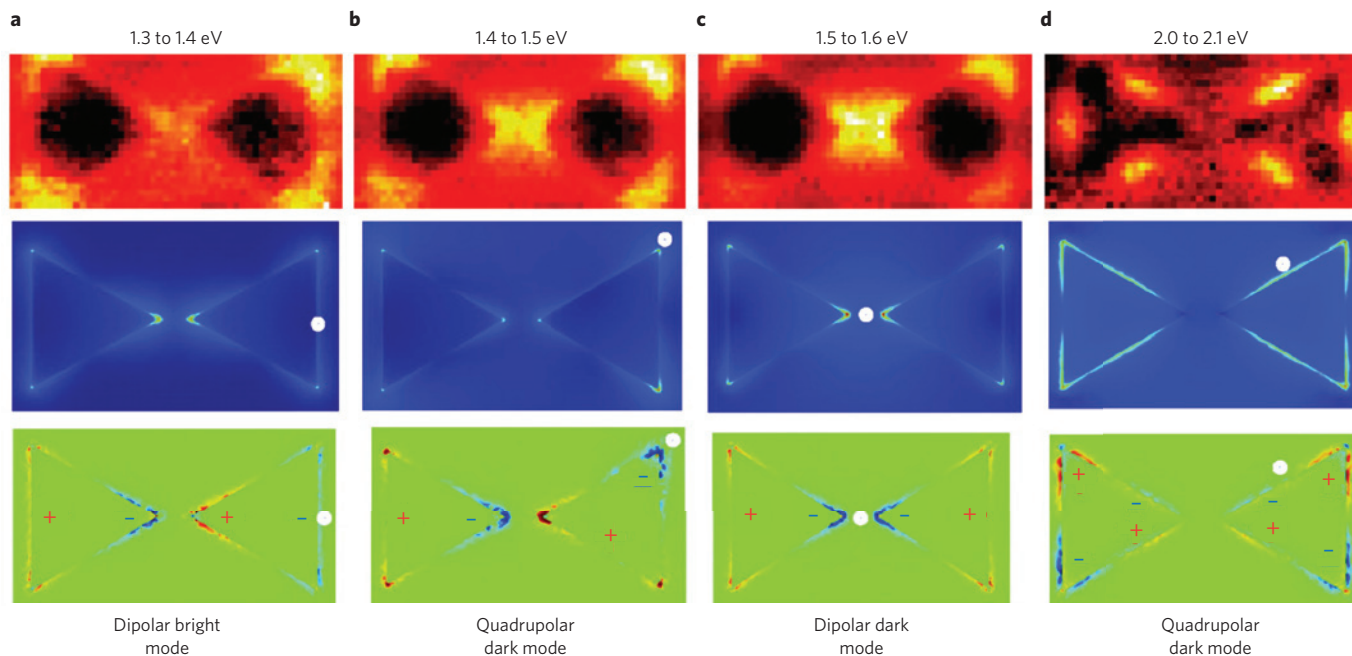


Figure 4 | Mapping of the modal spatial field distributions of the lowest-order bright and dark modes of gold bowtie nanoantennas. The total size of the nanoantenna is approximately 250 nm. **a–d**, Experimentally observed field distribution using electron energy-loss spectroscopy (EELS, top row), results from full-wave electromagnetic simulations of the EELS process (middle) and the corresponding charge distributions (bottom), clearly outlining the bright and dark character of the underlying modes. Figure reproduced with permission from ref. 68, © 2011 ACS.

all three directions, and a central objective is to efficiently and with low beam-divergence outcouple the coherent energy to the far-field continuum — similar to photonic lasers. In all three types of nanolasers (spasers, plasmon lasers and metamaterial lasers) the involvement of electrons in the surface plasmons adds momentum to the light, confining it tightly to the metal in one or more directions, and allowing for the build up of intense optical energy well below the diffraction barrier on extremely fast timescales^{32,39–41,65}, thereby extending the capabilities of laser systems in general. Remarkably, the sizes of these plasmon excitations are now tantalizingly close to those of solid-state electronic wavefunctions where such enhancements are optimal. Plasmon lasers could therefore be unique nanopropbes, providing enhanced sensitivity for single-molecule Raman^{75–78} and fluorescence^{79–81} spectroscopies, as well as nonlinear optics^{82–84}.

The first plasmon lasers utilized quite different metallic nanostructures. Hill and co-workers⁶¹ confined surface plasmons between the metal planes of an etched semiconductor heterostructure, as shown in Fig. 5a. The so-called metal–insulator–metal surface plasmons^{85,86} were also weakly confined by a small index variation along the heterostructure's growth direction, leading to guided-wave propagation parallel to the plane of the substrate. The end facets of the metallized structure completed a Fabry–Perot resonator. Another device reported by Oulton and co-workers⁶² also used a Fabry–Perot cavity, but this time with strong subwavelength confinement in two dimensions, perpendicular to wave propagation. The cavity consisted of a semiconductor nanowire sitting on a flat metal film with a thin nanoscale insulating gap (Fig. 5b). Here, the mode of the nanowire and the surface plasmon hybridize into a deep-subwavelength mode propagating along the wire's axis⁸⁷. Clearly, both of these plasmonic lasers generate optical energy principally bound to metal interfaces. In experiments, laser light in the far-field is only observed indirectly, through scattering.

Plasmon lasers constructed on the principle of a Fabry–Perot cavity around a plasmon waveguide will always be restricted to sub-diffraction limited confinement in one or two dimensions. Meanwhile, the basic building blocks of metamaterials are nanoparticles with subwavelength dimensions in all three dimensions

(Box 2). An electrically injected nanoparticle laser operating in the mid-infrared region shows tantalizing proof that such extreme laser cavities are possible⁸⁸. A number of reports of nanoparticle lasers at shorter wavelengths also suggest that amplification can compensate for the increasing absorptive loss^{89,90}. It is important to note however, that such nanoparticles are only subwavelength due to the dielectric materials that surround them. Resonant nanoparticles smaller than the diffraction limit in all three dimensions only occur near the metal's surface plasmon frequency, where interactions between light and electrons are strongest. Noginov and co-workers have reported such a device that consists of a dielectric clad with spherical silver particles measuring just 44 nm (ref. 63). Here, the localized surface plasmon of a 15-nm-diameter silver particle is amplified by dye molecules (OG 488) within a silica shell (Fig. 5c). The researchers report the signature of laser action under strong optical pumping. This is the only report of laser action at the surface plasmon frequency so far. However, the fact that the attained emission linewidth of about 6 nm was — even for the standards of plasmonic nanolasers — rather broad, and that the linewidth reduction while entering the laser-oscillation regime was not as pronounced as might ideally be expected^{51,91}, suggest that substantial room for improvement is available for follow-up works.

A point that should be highlighted in passing, concerns direct electrical (rather than optical) pumping of active semiconductor-based nanoplasmonic metamaterials and lasers. Although, as mentioned previously, electrical injection is highly preferred for many envisaged applications, it is not without caveats. A key aspect here is the current density required to overcome dissipative losses or to lead to full nanolasing. Owing to the plasmonic nature of the involved structures, the required injection current densities are high, particularly for subwavelength plasmonic particles having ultrasmall cross sections. These densities, which can be of the order of hundreds of kA cm^{-2} (ref. 92) can irreversibly heat and damage the fabricated structures. This may be one of the main reasons why, until now, attempts to demonstrate electrically pumped plasmonic nanolasers with truly subwavelength dimensions have met substantial challenges. With optical pumping, on the other hand, there is

the opportunity of using ultrashort light pulses (of femtosecond duration) that, being shorter than typical phonon timescales, allow for avoiding the generation of excessive heat. Clearly, such ultrashort excitation/pumping is challenging to achieve with electrical injection. However, the fact that metals are excellent heat sinks, capable of conducting heat efficiently, may allow for viable designs and for overcoming these challenges. To this end, nanoplasmonic metamaterial designs that are not restricted to being subwavelength in all three dimensions, but are ultrathin, flat and have high surface area through which heat may efficiently be conducted are particularly attractive.

The distinctions between plasmonic and photonic lasers are, as outlined previously, critically important when we consider gain instabilities in metamaterials. Although it is widely accepted that SE noise tends to accumulate near individual metallic nanoresonators, dense (for example, negative-index fishnet) optical metamaterials can allow for coherent interactions mediated through the coupling of their meta-atoms (Box 2), establishing global resonances that collectively provide internal feedback (see for example, Fig. 3). A crucial challenge that should be addressed here is that, depending on the coupling of the meta-atoms, random-phase emission could occur unless the emission band of the periodic metamaterial is designed to, for example, exhibit a sharp maximum (or minimum) at the $k = 0$ point for both in-plane directions and polarizations, favouring phase-locking.

At present there is a significant experimental effort underway to construct such a coherently emitting metamaterial^{39–41,49,93} — an ultrathin, large-area plasmonic amplifier that can couple strongly to the continuum, with low beam-divergence. Figure 6a shows an example of such a nanostructure, in which lead sulphide (PbS) semiconductor QDs were dispersed in polymethylmethacrylate (PMMA) and then spin coated onto a periodic array of asymmetric split-ring slits⁹³. The active metamaterial was pumped at 532 nm, and when the periodicity and dimensions of the slits were judiciously chosen such that the collective metamaterial (absorption)

resonance matched the QD emission wavelength around 1,300 nm (Fig. 6b), an eightfold enhancement of the photoluminescence peak was observed compared with the bare QD/PMMA layer (Fig. 6c). Simultaneously, a decrease of the full-width at half-maximum (FWHM) of the photoluminescence peak from 176 nm (without the metamaterial) to 100 nm (with the metamaterial) was reported. Both of these observations were shown to be consistent with the well-known cavity quantum electrodynamics (cQED) Purcell effect, according to which the SE in a cavity (here, an open metamaterial ‘cavity’) of volume V and quality factor Q can be enhanced by a factor of $F_p = [3/(4\pi^2)](\lambda/n_c)^3(Q/V)$, with n_c being the cavity refractive index.

Applications and outlook

Gain in metallic nanostructures is vital for realizing practical devices based on plasmonic and metamaterial principles⁹⁴. This Review has highlighted two regimes where gain could be utilized: first, in amplification mode, unique properties of metamaterials can be exploited while simultaneously compensating for loss; second, in lasing mode, feedback over the nanostructure could enable light sources with characteristics not achievable in conventional lasers.

One of the potential applications of gain media is to compensate for loss in negative-refractive-index metamaterials^{14,34}. Although claims^{54,55} that loss in these materials is unavoidable are unsound^{56,57}, it is the case in practice that loss can be a limiting factor⁹⁵. The so-called perfect lens¹³ achieves subwavelength resolution by exploiting resonant states in a negatively refracting material to amplify the near field in the image plane. Ultimately losses cut off this resonant amplification and hide the finer details in the image. Schemes have been discussed for incorporating gain material into the fabric of the lens itself³⁴, and tackling the losses at source. However, there is a more subtle way of achieving the same end. A theorem⁹⁶ states that if we take a slab of material defined by $\{\epsilon(x, y, z), \mu(x, y, z); 0 < z < d\}$, where ϵ and μ are the slab permittivity and slab permeability, respectively, and d is the slab width, then an adjacent slab

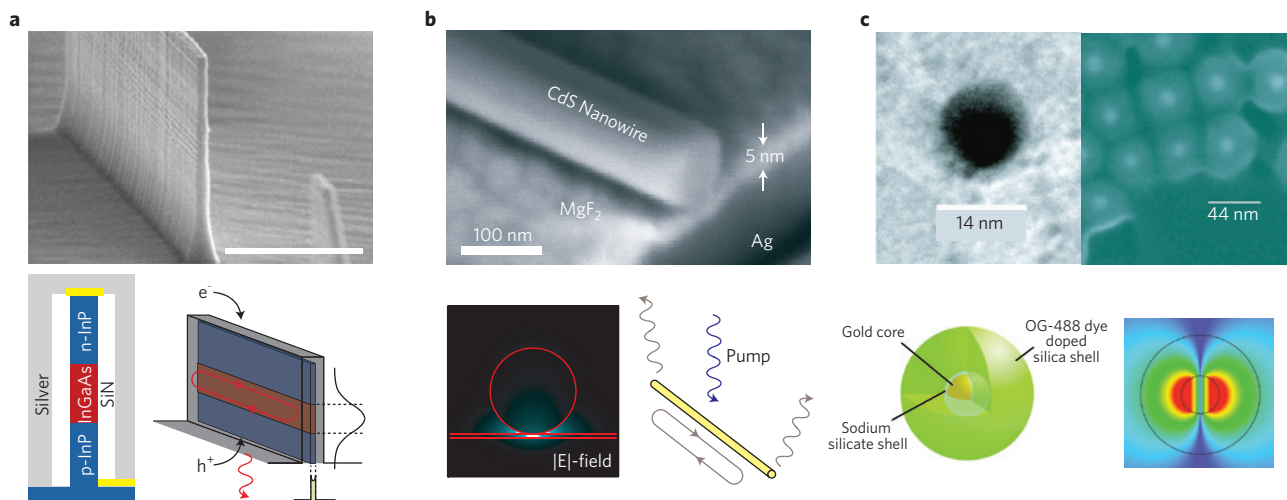


Figure 5 | Experimental demonstrations of plasmonic lasers exhibiting sub-diffraction limited confinement in one, two and three dimensions. a, Electron micrograph of a plasmonics laser with sub-diffraction limit confinement in one dimension (top, scale bar is 1,000 nm). Light is confined between two metal planes for gap widths as small as 100 nm at a wavelength near 1,500 nm (bottom right). Weaker confinement is along the semiconductor–heterostructure growth direction and reflection from the metal end-facets complete the Fabry–Perot cavity mode. Laser action occurs by electrically pumped recombination and gain within the semiconductor (bottom left), which is weakly scattered into the substrate. **b**, Here, a similar Fabry–Perot cavity design (top) is employed but now confinement is extremely strong in two dimensions due to the hybridization of the modes of semiconductor nanowire and metal surface (bottom left). Laser action occurs by optically pumped recombination and gain in the semiconductor nanowire, and are collected via weak light scattering from its end-facets (bottom right). **c**, Maximal confinement is achieved in metal nanoparticle lasers (top). In contrast to the Fabry–Perot approach, the nanoparticle design induces extremely strong feedback as it is much smaller than the wavelength (bottom left); instead cavity loss is dominated by electron scattering in the metal. Laser action arises from optically pumped emission and gain from dye molecules in an insulating shell around the metal particle (bottom right). Figure reproduced with permission from: **a**, ref. 61, © 2009 OSA; **b**, ref. 62, © 2009 NPG; **c**, ref. 63, © 2009 NPG.

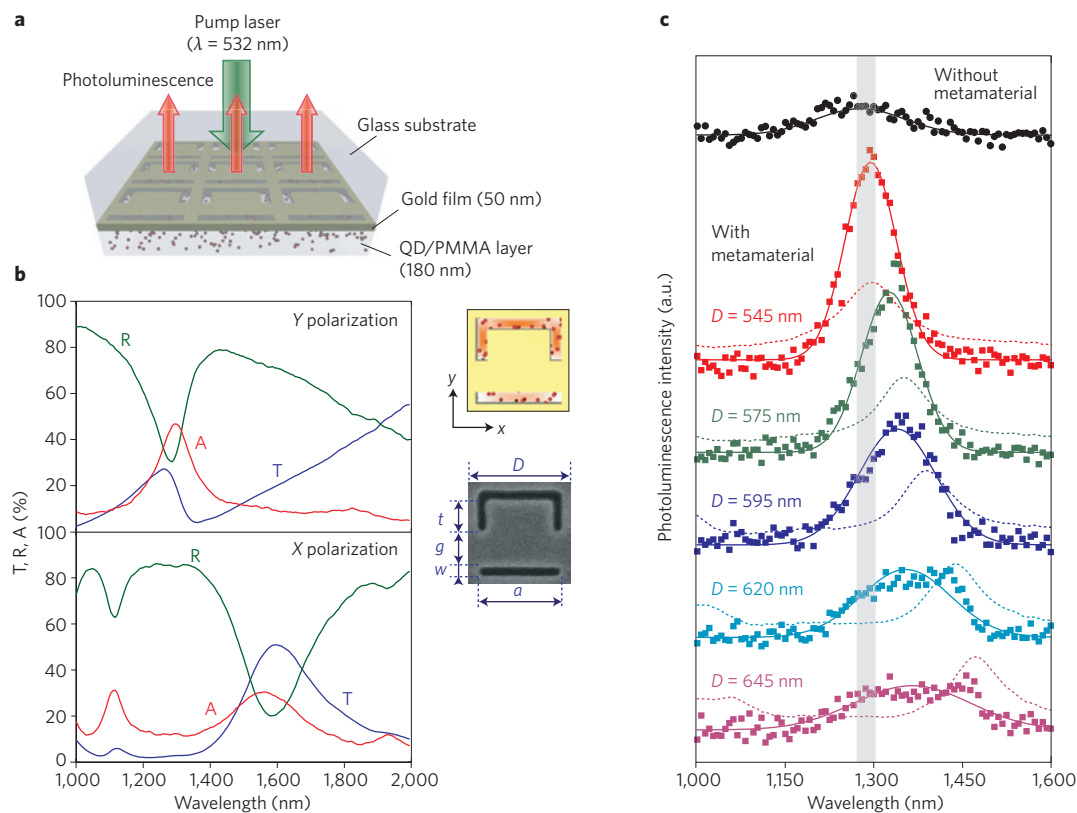


Figure 6 | Multifold enhancement of quantum-dot luminescence in plasmonic metamaterials. **a**, Schematic of the functionalized magnetic metamaterial made of a periodic array of asymmetric split-ring slits and a layer of QDs on top of it. Illumination is from the glass substrate. **b**, Measured transmission (blue), reflection (green) and absorption (red) coefficients of the active structure of a QD-coated metamaterial for E_y (top) and E_x (bottom) polarization. The two images to the right show (upper) a sketch of QDs in the resonant mode volume as seen from the substrate side, and (lower) a scanning electron micrograph of the metamaterial unit cell (without QDs). **c**, Photoluminescence spectra of the bare QD/PMMA layer (black) and of the periodic active nanostructure for different values of the unit-cell size D . Solid lines are Gaussian fits to the experimental results, whereas the dotted curves show the metamaterial's absorption spectra. The shaded area indicates the wavelength region where the photoluminescence of the QD/PMMA layer peaks ($\sim 1,280$ nm). Figure reproduced with permission from ref. 93, © 2010 APS.

of material defined by $\{-\epsilon(x, y, -z), -\mu(x, y, -z); -d < z < 0\}$ will completely compensate for the effect of the first slab and the effect of the two together will be as if neither were present: the second slab behaves like 'optical antimatter' and annihilates the first slab. This theorem works just as well if ϵ, μ are complex, that is, if one set is lossy material with negative real parts to ϵ, μ and the other a gain medium with positive real parts to ϵ, μ but negative imaginary parts. In this way, we envisage an object on one side of the pair of compensating slabs exactly reproduced on the other side as if nothing separated the two sides. This arrangement has the advantage of separating two complex operations: the creation of negative refraction and introduction of gain.

A potential use of metamaterials for constructing nanolasers is to exploit the extraordinarily strong dispersion in nanoplasmonic structures. For example, plasmonic and metamaterial waveguides feature zero-group-velocity (zero- v_g) points for modes characterized by a complex frequency (ω) and real wave-vector (k) (refs 15,97). These complex- ω modes are different from the complex- k /real- ω modes generally observed under coherent excitation, which do not preserve the zero- v_g point when the structure is lossy or active⁹⁷. Meanwhile, spontaneous recombination incoherently excites the complex- ω /real- k states. The zero- v_g points of these states are particularly interesting because they are regions of singular photonic density of states⁹⁸. An important current goal is hence to cleanly access such points⁹⁹, and thereby control SE, which is the chief limiting factor of the energy/noise performance and modulation bandwidth of (nano)lasers¹⁰⁰. At a zero- v_g point of an active plasmonic

nanostructure almost all SE is funnelled into a single 'stopped-light' mode, which greatly modifies the threshold characteristics. In this stopped-light regime, the 'cavity' can be completely open, and both low-threshold¹⁰⁰ and cavity-free lasing can occur. Preliminary Maxwell-Bloch analyses of complex- ω modes at the zero- v_g point of active plasmonic waveguides show that such a reduced-threshold, open-cavity lasing operation is a realistic possibility.

The incorporation of gain in metallic nanostructures has also found widespread interest in plasmonics, due to the potential for novel and unique optoelectronic capabilities. For example, the previously described plasmonic lasers could serve as sources of nanoscopic light for use in the near-field where strong light-matter interactions would allow for sensitive fluorescence or Raman spectroscopy at the single-molecule level^{101,102}. There is also considerable interest in loss compensation in plasmonic waveguides for routing optical signals in densely integrated circuits²⁸. This provides the capability to integrate amplification with other functionalities in a single component, thereby allowing more compact integration. Devices such as PlasMOSstor electro-optic modulators¹⁰³ could provide integrated amplification and switching functions (at present implemented by two independent components) within integrated nanocircuits.

Gain-enhanced metamaterials and nanoplasmonics constitute an exciting new frontier of nanoscience and technology, and are precursors towards active, integrated, quantum nano-optics. By manipulating and shaping the emission spectra of fluorescent elements on the tiniest scales (around or less than a few tens of nanometres), they

give rise to exceptionally fast nonlinearities, enabling nanoscopic amplifiers, lasers and sources of coherent optical energy, operating well below the diffraction limit of visible light. Although significant challenges, such as the control of the dissipated heat and the attainment of overall energy-efficient operation still remain, the fact that the sizes of the supported plasmonic excitations are already close to those of solid-state electronic wavefunctions promises that these components could provide unique sensitivity for single-emitter spectroscopy and super-resolution imaging. In this Review we have discussed and elucidated the intricate physics behind the interaction of plasmons with gain media, and summarized exemplary technological areas where the impact from this research at present is anticipated to be significant, although we anticipate that new ideas will also emerge about applications and future directions of this fertile field.

References

- Novotny, L. & Hecht, B. *Principles of Nano-Optics* (Cambridge Univ. Press, 2006).
- Maier, S. A. *Plasmonics: Fundamentals and Applications* (Springer, 2007).
- Fleischmann, M., Hendra, P. J. & McQuillan, A. J. Raman spectra of pyridine adsorbed at a silver electrode. *Chem. Phys. Lett.* **26**, 163–166 (1974).
- Jeanmaire, D. L., Van Duyne, R. P. & Sloan, A. P. Surface Raman spectroelectrochemistry: Part I. Heterocyclic, aromatic, and aliphatic amines adsorbed on the anodized silver electrode. *J. Electroanal. Chem.* **84**, 1–20 (1977).
- Albrecht, M. G. & Creighton, J. A. Anomalous intense Raman spectra of pyridine at a silver electrode. *J. Am. Chem. Soc.* **99**, 5215–5217 (1977).
- Ebbesen, T. W., Genet, C. & Bozhevolnyi, S. I. Surface-plasmon circuitry. *Phys. Today* **61**, 44–50 (May 2008).
- Barnes, W. L., Dereux, A. & Ebbesen, T. W. Surface plasmon subwavelength optics. *Nature* **424**, 824–830 (2003).
- Ozbay, E. Plasmonics: Merging photonics and electronics at nanoscale dimensions. *Science* **311**, 189–193 (2006).
- Novotny, L. & van Hulst, N. Antennas for light. *Nature Photon.* **5**, 83–90 (2011).
- Giannini, V. *et al.* Controlling light localization and light–matter interactions with nanoplasmons. *Small* **6**, 2498–2507 (2010).
- Cai, W. & Shalaev, V. M. *Optical Metamaterials: Fundamentals and Applications* (Springer, 2009).
- Shalaev, V. M. Optical negative-index metamaterials. *Nature Photon.* **1**, 41–48 (2007).
- Soukoulis, C. M., Linden, S. & Wegener, M. Negative refractive index at optical wavelengths. *Science* **315**, 47–49 (2007).
- Pendry, J. B. Negative refraction makes a perfect lens. *Phys. Rev. Lett.* **85**, 3966–3969 (2000).
- Tsakmakidis, K. L., Boardman, A. D. & Hess, O. ‘Trapped rainbow’ storage of light in metamaterials. *Nature* **450**, 397–401 (2007).
- Pendry, J. B., Schurig, D. & Smith, D. R. Controlling electromagnetic fields. *Science* **312**, 1780–1782 (2006).
- Leonhardt, U. Optical conformal mapping. *Science* **312**, 1777–1780 (2006).
- Gansel, J. K. *et al.* Gold helix photonic metamaterials as broadband circular polarizer. *Science* **325**, 1513–1515 (2009).
- Rose, A., Huang, D. & Smith, D. R. Controlling the second harmonic in a phase-matched negative-index metamaterial. *Phys. Rev. Lett.* **107**, 063902 (2011).
- Zharov, A. A., Shadrivov, I. V. & Kivshar, Y. S. Nonlinear properties of left-handed metamaterials. *Phys. Rev. Lett.* **91**, 037401 (2003).
- Maier, S. Plasmonic field enhancement and SERS in the effective mode volume picture. *Opt. Express* **14**, 1957–1964 (2006).
- Boardman, A. D. (ed.) *Electromagnetic Surface Modes* (Wiley, 1982).
- Raether, H. *Surface Plasmons on Smooth and Rough Surfaces and on Gratings* (Springer, 1988).
- Soukoulis, C. M. & Wegener, M. Optical metamaterials — more bulky and less lossy. *Science* **330**, 1633–1634 (2010).
- Boltasseva, A. & Atwater, H. A. Low-loss plasmonic metamaterials. *Science* **331**, 290–291 (2011).
- Anlage, S. M. The physics and applications of superconducting metamaterials. *J. Opt.* **13**, 024001 (2011).
- Chen, H-T. *et al.* Tuning the resonance in high-temperature superconducting terahertz metamaterials. *Phys. Rev. Lett.* **105**, 247402 (2010).
- Berini, P. & De Leon, I. Surface plasmon–polariton amplifiers and lasers. *Nature Photon.* **6**, 16–24 (2012).
- Soukoulis, C. M. & Wegener, M. Past achievements and future challenges in the development of three-dimensional photonic metamaterials. *Nature Photon.* **5**, 523–530 (2011).
- Barnes, W. L. Fluorescence near interfaces: the role of photonic mode density. *J. Mod. Opt.* **45**, 661–699 (1998).
- Ramakrishna, S. A. & Pendry, J. B. Removal of absorption and increase in resolution in a near-field lens via optical gain. *Phys. Rev. B* **67**, 201101(R) (2003).
- Bergman, D. J. & Stockman, M. I. Surface plasmon amplification by stimulated emission of radiation: quantum generation of coherent surface plasmons in nanosystems. *Phys. Rev. Lett.* **90**, 027402 (2003).
- Giannini, V., Fernández-Domínguez, A. I., Heck, S. C. & Maier, S. A. Plasmonic nanoantennas: fundamentals and their use in controlling the radiative properties of nanoemitters. *Chem. Rev.* **111**, 3888–3912 (2011).
- Xiao, S. *et al.* Loss-free and active optical negative-index metamaterials. *Nature* **466**, 735–738 (2010).
- Wuestner, S., Pusch, A., Tsakmakidis, K. L., Hamm, J. M. & Hess, O. Overcoming losses with gain in a negative refractive index metamaterial. *Phys. Rev. Lett.* **105**, 127401 (2010).
- Fang, A., Koschny, Th. & Soukoulis, C. M. Self-consistent calculations of loss-compensated fishnet metamaterials. *Phys. Rev. B* **82**, 121102(R) (2010).
- Wuestner, S., Pusch, A., Tsakmakidis, K. L., Hamm, J. M. & Hess, O. Gain and plasmon dynamics in active negative-index metamaterials. *Phil. Trans. R. Soc. A* **369**, 3525–3550 (2011).
- Hamm, J. M., Wuestner, S., Tsakmakidis, K. L. & Hess, O. Theory of light amplification in active fishnet metamaterials. *Phys. Rev. Lett.* **107**, 167405 (2011).
- Zheludev, N. I., Prosvirnin, S. L., Papasimakis, N. & Fedotov, V. A. Lasing spaser. *Nature Photon.* **2**, 351–354 (2008).
- Pusch, A., Wuestner, S., Hamm, J. M., Tsakmakidis, K. L. & Hess, O. Coherent amplification and noise in gain-enhanced nanoplasmonic metamaterials: A Maxwell-Bloch Langevin approach. *ACS Nano* **6**, 2420–2431 (2012).
- Wuestner, S. *et al.* Control and dynamic competition of bright and dark lasing states in active nanoplasmonic metamaterials. *Phys. Rev. B* **85**, 201406(R) (2012).
- Valentine, J. *et al.* Three-dimensional optical metamaterials with a negative refractive index. *Nature* **455**, 376–379 (2008).
- Zhang, S. *et al.* Near-infrared double negative metamaterials. *Opt. Express* **13**, 4922–4930 (2005).
- Hur, K. *et al.* Three-dimensionally isotropic negative refractive index materials from block copolymer self-assembled chiral gyroid networks. *Angew. Chem. Int. Ed.* **50**, 11985–989 (2011).
- Hess, O. & Gehrig, E. *Photonics of Quantum-Dot Nanomaterials and Devices: Theory and Modelling* (Imperial College Press, 2011).
- Böhringer, K. & Hess, O. A full time-domain approach to spatio-temporal dynamics of semiconductor lasers: I. theoretical formulation. *Prog. Quantum Electron.* **32**, 159–246 (2008).
- Böhringer, K. & Hess, O. A full time-domain approach to spatio-temporal dynamics of semiconductor lasers: II. spatio-temporal dynamics. *Prog. Quantum Electron.* **32**, 247–307 (2008).
- Cook, J. J. H., Tsakmakidis, K. L. & Hess, O. Ultralow-loss optical diamagnetism in silver nanoforests. *J. Opt. A* **11**, 114026 (2009).
- Meinzer, N. *et al.* Arrays of Ag split-ring resonators coupled to InGaAs single-quantum-well gain. *Opt. Express* **18**, 24140–24151 (2010).
- Smith, D. R., Schultz, S., Markoš, P. & Soukoulis, C. M. Determination of effective permittivity and permeability of metamaterials from reflection and transmission coefficients. *Phys. Rev. B* **65**, 195104 (2002).
- Stockman, M. I. The spaser as a nanoscale quantum generator and ultrafast amplifier. *J. Opt.* **12**, 024004 (2010).
- Rockstuhl, C. *et al.* Resonances of split-ring resonator metamaterials in the near infrared. *Appl. Phys. B* **84**, 219–227 (2006).
- Husnik, M. *et al.* Absolute extinction cross-section of individual magnetic split-ring resonators. *Nature Photon.* **2**, 614–617 (2008).
- Stockman, M. I. Criterion for negative refraction with low optical losses from a fundamental principle of causality. *Phys. Rev. Lett.* **98**, 177404 (2007).
- Stockman, M. I. Spaser action, loss-compensation, and stability in plasmonic systems with gain. *Phys. Rev. Lett.* **106**, 156802 (2011).
- Wuestner, S., Pusch, A., Tsakmakidis, K. L., Hamm, J. M. & Hess, O. Comment on ‘Spaser action, loss-compensation, and stability in plasmonic systems with gain’. *Phys. Rev. Lett.* **107**, 259701 (2011).
- Pendry, J. B. & Maier, S. A. Comment on ‘Spaser action, loss-compensation, and stability in plasmonic systems with gain’. *Phys. Rev. Lett.* **107**, 259703 (2011).
- De Leon, I. & Berini, P. Amplification of long-range surface plasmons by a dipolar gain medium. *Nature Photon.* **4**, 382–387 (2010).
- Gather, M. C., Meerholz, K., Danz, N. & Leosson, K. Net optical gain in a plasmonic waveguide embedded in a fluorescent polymer. *Nature Photon.* **4**, 457–461 (2010).
- Sorger, V. J. *et al.* Experimental demonstration of low-loss optical waveguiding at deep sub-wavelength scales. *Nature Commun.* **2**, 331 (2011).
- Hill, M. T. *et al.* Lasing in metal-insulator-metal sub-wavelength plasmonic waveguides. *Opt. Express* **17**, 11107–11112 (2009).

62. Oulton, R. F. *et al.* Plasmon lasers at deep-subwavelength scale. *Nature* **461**, 629–632 (2009).
63. Noginov, M. A. *et al.* Demonstration of a spaser-based nanolaser. *Nature* **460**, 1110–1112 (2009).
64. Ma, R.-M., Oulton, R. F., Sorger, V. J., Bartal, G. & Zhang, X. Room-temperature sub-diffraction-limited plasmon laser by total internal reflection. *Nature Mater.* **10**, 110–113 (2011).
65. Genov, D. A., Oulton, R. F., Bartal, G. & Zhang, X. Anomalous spectral scaling of light emission rates in low-dimensional metallic nanostructures. *Phys. Rev. B* **83**, 245312 (2011).
66. Vogelgesang, R. & Dmitriev, A. Real-space imaging of nanoplasmonic resonances. *Analyst* **135**, 1175–1181 (2010).
67. Sonnefraud, Y., Koh, A. L., McComb, D. W. & Maier, S. A. Nanoplasmonics: engineering and observation of localized plasmon modes. *Laser Photon. Rev.* **6**, 277–295 (2011).
68. Koh, A. L., Fernández-Domínguez, A. I., McComb, D. W., Maier, S. A. & Yang, J. K. W. High-resolution mapping of electron-beam-excited plasmon modes in lithographically defined gold nanostructures. *Nano Lett.* **11**, 1323–1330 (2011).
69. Prodan, E., Radloff, C., Halas, N. & Nordlander, P. A hybridization model for the plasmon response of complex nanostructures. *Science* **302**, 419–422 (2003).
70. Ringler, M. *et al.* Shaping emission spectra of fluorescent molecules with single plasmonic nanoresonators. *Phys. Rev. Lett.* **100**, 203002 (2008).
71. Kéna-Cohen, S. *et al.* Plasmonic sinks for the selective removal of long-lived states. *ACS Nano* **5**, 9958–9965 (2011).
72. Luk'yanchuk, B. *et al.* The Fano resonance in plasmonic nanostructures and metamaterials. *Nature Mater.* **9**, 707–715 (2010).
73. Giannini, V., Francescato, Y., Amrania, H., Phillips, C. C. & Maier, S. A. Fano resonances in nanoscale plasmonic systems: a parameter-free modelling approach. *Nano Lett.* **11**, 2835–2840 (2011).
74. Francescato, Y., Giannini, V. & Maier, S. A. Plasmonic systems unveiled by Fano resonances. *ACS Nano* **6**, 1830–1838 (2012).
75. Nie, S. & Emory, S. R. Probing single molecules and single nanoparticles by surface-enhanced Raman scattering. *Science* **275**, 1102–1106 (1997).
76. Anker, J. N. *et al.* Biosensing with plasmonic nanosensors. *Nature Mater.* **7**, 442–453 (2008).
77. Kneipp, K. *et al.* Single molecule detection using surface-enhanced Raman scattering (SERS). *Phys. Rev. Lett.* **78**, 1667–1670 (1997).
78. Hill, R. T. *et al.* Leveraging nanoscale plasmonic modes to achieve reproducible enhancement of light. *Nano Lett.* **10**, 4150–4154 (2010).
79. Anger, P., Bharadwaj, P. & Novotny, L. Enhancement and quenching of single-molecule fluorescence. *Phys. Rev. Lett.* **96**, 113002 (2006).
80. Liebermann, T. & Knoll, W. Surface-plasmon field-enhanced fluorescence spectroscopy. *Colloid Surf.* **171**, 115–130 (2000).
81. Kinkhabwala, A. *et al.* Large single-molecule fluorescence enhancements produced by bowtie nanoantenna. *Nature Photon.* **3**, 654–657 (2009).
82. Kano, H. & Kawata, S. Two-photon-excited fluorescence enhanced by a surface plasmon. *Opt. Lett.* **21**, 1848–1850 (1996).
83. Palomba, S. & Novotny, L. Nonlinear excitation of surface plasmon polaritons by four-wave mixing. *Phys. Rev. Lett.* **101**, 056802 (2008).
84. Danckwerts, M. & Novotny, L. Optical frequency mixing at coupled gold nanoparticles. *Phys. Rev. Lett.* **98**, 026104 (2007).
85. Dionne, J. A., Lezec, H. J. & Atwater, H. A. Highly confined photon transport in subwavelength metallic slot waveguides. *Nano Lett.* **6**, 1928–1932 (2006).
86. Dionne, J. A., Sweatlock, L. A., Atwater, H. & Polman, A. Plasmon slot waveguides: towards chip-scale propagation with subwavelength-scale localization. *Phys. Rev. B* **73**, 035407 (2006).
87. Oulton, R. F., Sorger, V. J., Genov, D. A., Pile, D. F. P. & Zhang, X. A hybrid plasmonic waveguide for subwavelength confinement and long-range propagation. *Nature Photon.* **2**, 496–500 (2008).
88. Walther, C., Scalari, G., Amanti, M. I., Beck, M. & Faist, J. Microcavity laser oscillating in a circuit-based resonator. *Science* **327**, 1495–1497 (2010).
89. Yu, K., Lakhani, A. M. & Wu, M. C. Subwavelength metal-optic semiconductor nanopatch lasers. *Opt. Express* **18**, 8790–8799 (2010).
90. Nezhad, M. P. *et al.* Room-temperature subwavelength metallo-dielectric lasers. *Nature Photon.* **4**, 395–399 (2010).
91. Ma, R.-M., Oulton, R. F., Sorger, V. J. & Zhang, X. Plasmon lasers: coherent light source at molecular scales. *Laser Photon. Rev.* <http://dx.doi.org/10.1002/lpor.201100040> (2012).
92. Khurgin, J. B. & Sun, G. Practicality of compensating the loss in plasmonic waveguides using semiconductor gain medium. *Appl. Phys. Lett.* **100**, 011105 (2012).
93. Tanaka, K., Plum, E., Ou, J. Y., Uchino, T. & Zheludev, N. I. Multifold enhancement of quantum dot luminescence in plasmonic metamaterials. *Phys. Rev. Lett.* **105**, 227403 (2010).
94. Zheludev, N. I. The road ahead for metamaterials. *Science* **328**, 582–583 (2010).
95. Smith, D. R. *et al.* Limitations on subdiffraction imaging with a negative refractive index slab. *Appl. Phys. Lett.* **82**, 1506–1508 (2003).
96. Pendry, J. B. & Ramakrishna, S. A. Focusing light using negative refraction. *J. Phys. Condens. Matter* **14**, 6345–6364 (2003).
97. Kirby, E. I., Hamm, J. M., Pickering, T. W., Tsakmakidis, K. L. & Hess, O. Evanescent gain for slow and stopped light in negative refractive index heterostructures. *Phys. Rev. B* **84**, 041103(R) (2011).
98. Tsakmakidis, K. L. & Hess, O. Extreme control of light in metamaterials: complete and loss-free stopping of light. *Physica B* <http://dx.doi.org/10.1016/j.physb.2012.01.093> (2012).
99. Jacob, Z. & Shalae, V. M. Plasmonics goes quantum. *Science* **334**, 463–464 (2011).
100. Yamamoto, Y. & Slusher, R. E. Optical processes in microcavities. *Phys. Today* **46**, 66–73 (June 1993).
101. Oulton, R. F. Surface plasmon lasers: sources of nanoscopic light. *Mater. Today* **15**, 592–600 (January–February 2012).
102. Sorger, V. J. *et al.* Strongly enhanced molecular fluorescence inside a nanoscale waveguide gap. *Nano Lett.* **11**, 4907–4911 (2011).
103. Dionne, J. A., Diest, K., Sweatlock, L. A. & Atwater, H. A. PlasMOSstor: a metal-oxide-Si field effect plasmonic modulator. *Nano Lett.* **9**, 897–902 (2009).

Additional information

The authors declare no competing financial interests. Reprints and permission information is available online at <http://www.nature.com/reprints>. Correspondence should be addressed to O.H.